Incommensurate strain-induced ordering of interstitial oxygen in Nb

2008 J. Phys.: Condens. Matter 20 275206

(http://iopscience.iop.org/0953-8984/20/27/275206)

J. Phys.: Condens. Matter **20** (2008) 275206 (5pp) doi:10.1088/0953-8984/20/27/275206

Incommensurate strain-induced ordering of interstitial oxygen in Nb

R P Kurta, V N Bugaev, A Stierle and H Dosch

Max-Planck-Institut für Metallforschung, Heisenbergstraße 3, D-70569 Stuttgart, Germany

E-mail: kurta@mf.mpg.de and vbugaev@mf.mpg.de

Received 17 March 2008, in final form 6 May 2008
Published 3 June 2008
Online at stacks.iop.org/JPhysCM/20/275206

Abstract

We present a semi-phenomenological theory of the strain-induced interaction between interstitial oxygen dissolved in Nb and predict an incommensurate oxygen ordering wave which is mediated by the intrinsic bcc instability at $\boldsymbol{k} = 2/3(111)$. We discuss the stability range of this ordering phenomenon, which may play a role in the performance of Nb radio frequency (RF) cavities for high energy particle accelerators.

(Some figures in this article are in colour only in the electronic version)

1. Introduction

One of the most advanced current applications of niobium is in the superconducting RF cavities of modern linear electron accelerators. The materials science challenge is to improve the high frequency superconducting performance such that highest field gradients are possible in order to achieve short acceleration distances and thus save costs. In recent years it has been discovered that electric field gradients up to and beyond 35 MV m^{-1} are possible by a surface annealing of the Nb cavities [1, 2]. While it is still unclear on the microscopic level what structural changes are induced upon annealing, it is assumed that oxygen and its redistribution at the surface and in the subsurface region plays a crucial role [3].

This theoretical work has been triggered by the results of a recent *in situ* x-ray diffraction study of the different Nb-oxide layers as they emerge and disappear at different annealing conditions [4]. A particularly interesting aspect has been the detection of atomar oxygen which is injected into the interstitial Nb lattice from the dissolving Nb-oxide layers (figure 1). It is well known that the presence of defects deteriorates the superconducting properties of Nb and by this the performance of the niobium cavities (see e.g. [5]). Interstitial oxygen has a particularly large effect, decreasing the superconducting transition temperature by 0.93 K per at.% and increasing the resistivity in the normal state by 5.2 $\mu\Omega$ cm per at.% [6].

At low concentrations, interstitial oxygen is disordered in the interstitial Nb lattice. However, above a certain concentration, oxygen can form a sequence of ordered phases [7, 8]. A possible ordering force is mediated by the static lattice distortions around the oxygen defect, as shown theoretically using a simple model for the local lattice distortions description [9]. We address here a new ordering mechanism for subsurface interstitial oxygen exploiting a more elaborated model of the local lattice distortions which has been proposed [10, 11] from a detailed analysis of diffuse neutron scattering data in NbO_x (this will be discussed in more detail in what follows).

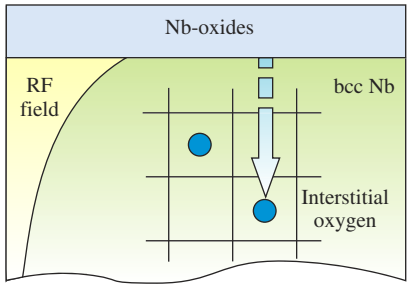

Figure 1. RF field decay in Nb and subsurface interstitial oxygen.

Interstitial oxygen is dissolved in bcc metals (like Nb) on so-called octahedral sites (figure 2) thereby inducing distortions ($\boldsymbol{U}^p(\boldsymbol{R})$) in the local lattice neighbourhood. They can very elegantly be modelled by so-called elastic ('Kanzaki') forces $\boldsymbol{F}^p(\boldsymbol{R})$ [12] which act on the Nb atoms around the first neighbour shells of the interstitial sublattice p (see figure 2),

$$\boldsymbol{U}^p(\boldsymbol{R}) = \sum_{\boldsymbol{R}'} \boldsymbol{G}(\boldsymbol{R}, \boldsymbol{R}')\boldsymbol{F}^p(\boldsymbol{R}'), \qquad (1)$$

with $\boldsymbol{G}(\boldsymbol{R}, \boldsymbol{R}')$ as the lattice Green function (see e.g. [13]).

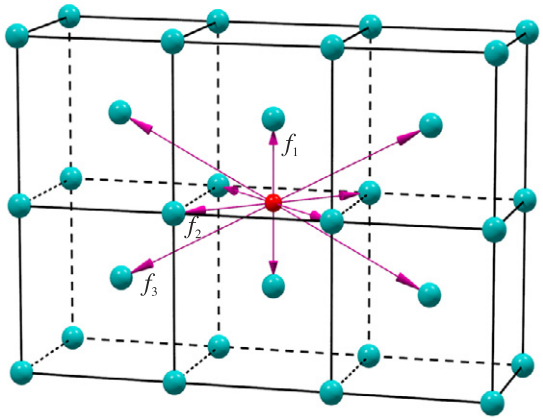

Figure 2. Kanzaki forces around one octahedral O interstitial acting on the first-(f_1), second-(f_2) and third-(f_3) nearest Nb neighbour atoms (note that only four (out of eight) third-nearest-Nb neighbour atoms are shown).

These defect-induced static distortions are very strong in the local neighbourhood, typically 0.1 − 0.5 Å, and exhibit a long ranging power-law decay ($1/r^2$) with distance r. The resulting lattice expansion with oxygen concentration c (at.%), $\Delta a/a = 0.126c$ [14], is directly related to the strength of the long-ranged part of the displacement field by the relation

$$\frac{\Delta a}{a} = \frac{cP}{\Omega_0(C_{11} + 2C_{12})}, \tag{2}$$

where P is the defect strength, 22.6 eV in the case of O in Nb [10], C_{ij} are the elastic constants and Ω_0 is the volume per atom.

The simplest Kanzaki force model which is consistent with this experimental value and the octahedral symmetry of the defect site requires elastic forces on the first and second neighbour shell ('2f model'). The associated long-ranged distortions give rise to an attractive interaction between two nearest oxygen defects. The strain-induced interaction was calculated based on this 2f model and concluded [9] that a commensurate ordered oxygen structure is stabilized with a wavevector $\boldsymbol{k} = (1/2, 1/2, 0)$ (see below).

In a detailed experimental and theoretical study of the diffuse neutron scattering in $NbO_{0.02}$ the very local lattice distortions around interstitial oxygen were determined and it was discovered that they are inconsistent with the 2f model [10, 11]. Instead, the local lattice displacements couple very strongly to the intrinsic bcc instability of Nb which is manifested by the pronounced soft phonon at $\boldsymbol{k} = 2/3(1, 1, 1)$. The local lattice distortions around interstitial oxygen can be understood as a local freezing of the soft 2/3(111) LA mode around the oxygen defect, giving rise to a static local fluctuation of the so-called ω-phase. Within the Kanzaki force approach, these ω-like local distortions require elastic forces up to the third neighbour shell ('3f model') [10, 11]. In what follows we show—using the static concentration wave approach [15]—that these ω-type distortions give rise to pronounced incommensurate ordering waves of the interstitial oxygen. We also show that this incommensurate ordered structure is more stable than the commensurate order predicted in [9].

2. Theoretical background

The strain-induced pairwise interaction energy $V^{\rm si}_{pq}(\boldsymbol{R})$ between interstitials at positions p and q in two unit cells separated by the translation vector $\boldsymbol{R}$ is given by

$$V^{\rm si}_{pq}(\boldsymbol{R}) = \frac{1}{N}\sum_{\boldsymbol{k}} V^{\rm si}_{pq}(\boldsymbol{k})\mathrm{e}^{-\mathrm{i}\boldsymbol{k}\boldsymbol{R}}, \tag{3}$$

where the summation is carried out over the first Brillouin zone. $V^{\rm si}_{pq}(\boldsymbol{k})$ is the Fourier component of the interaction energy which reads [15]:

$$V^{\rm si}_{pq}(\boldsymbol{k}) = -\boldsymbol{F}_p(\boldsymbol{k})\boldsymbol{G}(\boldsymbol{k})\boldsymbol{F}^*_q(\boldsymbol{k}) + Q_{pp}\delta_{pq} \qquad (\boldsymbol{k} \neq 0), \tag{4}$$

$$Q_{pp} = \frac{1}{N}\sum_{\boldsymbol{k}} \boldsymbol{F}_p(\boldsymbol{k})\boldsymbol{G}(\boldsymbol{k})\boldsymbol{F}^*_p(\boldsymbol{k}). \tag{5}$$

Q_{pp} is introduced in order to exclude the so-called 'self-action' [15]. In equations (4) and (5) $\boldsymbol{F}_p(\boldsymbol{k})$ is a Fourier component of the Kanzaki force $\boldsymbol{F}_p(\boldsymbol{R})$ and $\boldsymbol{G}(\boldsymbol{k})$ is the Fourier transform of the lattice Green function $\boldsymbol{G}(\boldsymbol{R}, \boldsymbol{R}')$, which is usually obtained via a Born–von Kármán fit to the phonon spectrum [16, 17].

Within the mean-field approximation, the configurational energy of the interstitial alloy in terms of the pairwise interaction energies is [15, 18]

$$E = \tfrac{1}{2}\sum_{p,q}\sum_{\boldsymbol{R},\boldsymbol{R}'} V^{\rm tot}_{pq}(\boldsymbol{R} - \boldsymbol{R}')n(p, \boldsymbol{R})n(q, \boldsymbol{R}'), \tag{6}$$

where the summation is carried out over all interstitial sites $\{p, \boldsymbol{R}\}$ and $\{q, \boldsymbol{R}'\}$. The quantity $n(p, \boldsymbol{R})$ is the occupation probability of finding an interstitial atom in the $(p, \boldsymbol{R})$ interstitial site, and $V^{\rm tot}_{pq}(\boldsymbol{R} - \boldsymbol{R}')$ is the total interaction energy of a pair of interstitials located at the interstitial sites $(p, \boldsymbol{R})$ and $(q, \boldsymbol{R}')$. The total interaction energy $V^{\rm tot}_{pq}$ between two oxygen defects can be represented as a sum of two contributions, the short-ranged chemical interaction $V^{\rm ch}_{pq}$ determined in the undistorted lattice and the strain-induced interaction $V^{\rm si}_{pq}$ mediated by the lattice relaxation [15],

$$V^{\rm tot}_{pq}(\boldsymbol{R} - \boldsymbol{R}') = V^{\rm si}_{pq}(\boldsymbol{R} - \boldsymbol{R}') + V^{\rm ch}_{pq}(\boldsymbol{R} - \boldsymbol{R}'). \tag{7}$$

It is convenient to represent the occupation numbers $\{n(p, \boldsymbol{R})\}$ in terms of the amplitudes $\{\gamma_\sigma(\boldsymbol{k})\}$ of the orthonormal set of concentration waves. After diagonalizing the matrix $\boldsymbol{V}^{\rm tot}(\boldsymbol{R} - \boldsymbol{R}')$ in (6), one obtains[1] [15]

$$E = \tfrac{1}{2}\sum_{\sigma,s} \lambda_\sigma(\boldsymbol{k}_{\rm s})\Gamma_{\sigma,s}\eta^2_{\sigma,s}, \tag{8}$$

$$\Gamma_{\sigma,s} = \sum_j |\gamma_\sigma(\boldsymbol{k}_{j_{\rm s}})|^2, \tag{9}$$

[1] In (8) the summation is carried out over all waves $\{\sigma, \boldsymbol{k}_{\rm s}\}$, where 's' determines the star of the wavevectors, and the summation in (9) is carried out over the vectors $j_{\rm s}$ belonging to the same star 's'.

Table 1. Two models of the Kanzaki forces for O in Nb.

Kanzaki forces (eV Å^{-1})	2f model [22]	3f model [10, 11]
f_1	3.63	2.80
f_2	1.06	−0.27
f_3	0	0.54

where $\eta_{\sigma,s}$ is the standard long-range order parameter and $\lambda_\sigma(\boldsymbol{k})$ are the eigenvalues of the $V^{\rm tot}_{pq}(\boldsymbol{k})$ matrix, which can be determined from the secular equation

$$\sum_{q=1}^{\nu} V^{\rm tot}_{pq}(\boldsymbol{k})\upsilon_\sigma(q,\boldsymbol{k}) = \lambda_\sigma(\boldsymbol{k})\upsilon_\sigma(p,\boldsymbol{k}). \tag{10}$$

The 'polarization vectors' $\upsilon_\sigma(p,\boldsymbol{k})$ are the eigenvectors of the matrix $V^{\rm tot}_{pq}(\boldsymbol{k})$, the 'polarization number' σ designates one of the ν branches[2] of the spectrum $\lambda_\sigma(\boldsymbol{k})$.

From equation (8) one concludes that the structure of the most stable ordered phase is determined by the star $\boldsymbol{k}^{\rm min}_{\rm s}$, whose wavevectors $\{\boldsymbol{k}^{\rm min}_{j_s}\}$ and polarization vectors $\{\upsilon^{\rm min}_\sigma(p,\boldsymbol{k}^{\rm min}_{j_s})\}$ provide the absolute minimum of $\lambda_\sigma(\boldsymbol{k}_{\rm s})$ [15]. The occupation probability function $n(p,\boldsymbol{R})$, which describes the atomic distribution in such an ordered phase, is defined as a superposition of static concentration waves [15]:

$$n(p,\boldsymbol{R}) = c + \sum_s \sum_{\sigma=1}^{\nu} \eta_\sigma \sum_{\boldsymbol{k}^{\rm min}_{j_s}} \gamma_\sigma(\boldsymbol{k}^{\rm min}_{j_s})\upsilon_\sigma(p,\boldsymbol{k}^{\rm min}_{j_s}) {\rm e}^{{\rm i}\boldsymbol{k}^{\rm min}_{j_s}\boldsymbol{R}}, \tag{11}$$

where c is a concentration of the interstitial atoms. A detailed description of the static concentration wave approach can be found elsewhere (e.g. [15, 19, 20]).

3. Results and discussion

The Nb–O solid solution is composed of the bcc host lattice and three interpenetrating bcc sublattices of the octahedral interstitial sites ($p, q = 1, 2, 3$) which are occupied by oxygen atoms. The position of any interstitial $(p,\boldsymbol{R})$ is defined by a vector

$$\boldsymbol{R}_p = \boldsymbol{R} + \boldsymbol{h}_p, \tag{12}$$

where $\boldsymbol{h}_p$ is the vector separating the interstitial from the host atom in the unit cell $\boldsymbol{R}$. In the case of the Nb–O solid solution, the vectors $\boldsymbol{h}_p$ have the coordinates

$$\boldsymbol{h}_1 = a_0\left(\tfrac{1}{2},0,0\right), \qquad \boldsymbol{h}_2 = a_0\left(0,\tfrac{1}{2},0\right), \qquad \boldsymbol{h}_3 = a_0\left(0,0,\tfrac{1}{2}\right) \tag{13}$$

(a_0 is the lattice constant of Nb). The pairwise energies $V^{\rm si}_{pq}(\boldsymbol{r})$ of the strain-induced interaction of O interstitials and the eigenvalues $\lambda_\sigma(\boldsymbol{k})$ of the matrices $V^{\rm si}_{pq}(\boldsymbol{k})$ are calculated according to (3)–(5) and (10). The Green function $\boldsymbol{G}(\boldsymbol{R},\boldsymbol{R}')$ used in our calculations is based on the set of Born–von Kármán force constants taken from [21]. For our calculations we used the '3f model' and compared the results with ones from the '2f model'. The forces for the two used models are given in table 1.

[2] ν is equal to the number of interstitial sublattices, e.g. in the case of the Nb–O solid solution $\nu = 3$.

Table 2. The strain-induced pairwise interaction energies $V^{\rm si}_{pq}(\boldsymbol{r})$ (eV) between O interstitials separated by $\boldsymbol{r}$.

	$V^{\rm si}$ [eV]			$V^{\rm si}$ [eV]	
$\boldsymbol{r}$	2f model	3f model	$\boldsymbol{r}$	2f model	3f model
$(0,\frac{1}{2},0)$	−0.826	0.668	(1,1,1)	−0.033	−0.069
$(\frac{1}{2},0,\frac{1}{2})$	−0.077	−0.481	$(1,\frac{3}{2},0)$	0.007	−0.028
$(\frac{1}{2},\frac{1}{2},\frac{1}{2})$	−0.248	−0.119	$(\frac{3}{2},1,\frac{1}{2})$	0.025	−0.017
(0, 0, 1)	1.099	0.713	(2, 0, 0)	−0.035	0.046
(1, 0, 0)	0.018	−0.336	(0, 0, 2)	0.340	0.253
$(1,\frac{1}{2},0)$	0.126	−0.207	$(2,\frac{1}{2},0)$	−0.018	−0.064
$(\frac{1}{2},1,\frac{1}{2})$	−0.043	0.047	$(1,\frac{3}{2},1)$	−0.021	0.039
(1, 1, 0)	0.128	0.110	$(\frac{1}{2},2,\frac{1}{2})$	−0.005	0.025
(1, 0, 1)	−0.123	0.066	$(\frac{3}{2},0,\frac{3}{2})$	0.011	0.017
$(1,\frac{1}{2},1)$	0.017	−0.026	$(\frac{3}{2},\frac{3}{2},\frac{1}{2})$	0.022	0.032
$(0,\frac{3}{2},0)$	−0.067	−0.081	$(\frac{3}{2},\frac{1}{2},\frac{3}{2})$	−0.042	0.001
$(\frac{1}{2},0,\frac{3}{2})$	−0.045	0.145	(2, 1, 0)	−0.018	−0.003
$(\frac{3}{2},\frac{1}{2},\frac{1}{2})$	0.008	−0.075	(0, 1, 2)	−0.006	0.028
$(\frac{1}{2},\frac{1}{2},\frac{3}{2})$	0.044	−0.021	(2, 0, 1)	0.017	0.014

Table 2 summarizes the obtained strain-induced pairwise interaction energies $V^{\rm si}_{pq}(\boldsymbol{r})$ (eV) between two O interstitials located at $\boldsymbol{R}_p = (0,0,1/2)$ and at an arbitrary position $(q,\boldsymbol{R}')$, respectively, separated by a vector $\boldsymbol{r} = \boldsymbol{R}'_q - \boldsymbol{R}_p$.

Notice that the energies calculated within the 2f model are significantly different from the ones deduced from the 3f model. In figures 3(*a*) and (*b*) the eigenvalue spectra associated with the 2f and the 3f force model are plotted along the high symmetry directions. Our '2f' calculations reproduce the previous conclusions [9], i.e. an ordering wave with $\boldsymbol{k} = (1/2,1/2,0)$ and polarization vector $\upsilon_1(p,\boldsymbol{k}) = 1/\sqrt{2}(1,1,0)$. Not unexpectedly, the eigenvalue spectrum associated with the 3f model deviates significantly from the 2f results and predicts a new pronounced minimum near the incommensurate position $\boldsymbol{k} = (2/3,2/3,2/3)$. Interstitial oxygen thus exhibits a strong trend to order with an ordering wave which is intimately coupled to the soft LA 2/3(111) phonon.

In the search for the possible ordered phases, the set $\{\boldsymbol{k}_{\rm s}\} = \{\frac{2}{3}\,\frac{2}{3}\,\frac{2}{3}\}$ and the corresponding sets of the polarization vectors $\{\upsilon_\sigma(p,\boldsymbol{k}_{\rm s})\}$ obtained from (10) were used to determine the parameters of the distribution function (11) [19, 23, 24]. This comprehensive search resulted in only one possible superstructure characterized by an ordering wave with the polarization vector $\upsilon_1(p,\boldsymbol{k}) = 1/\sqrt{3}(1,1,1)$:

$$n(p,\boldsymbol{R}) = \begin{cases} \dfrac{1}{3} + \dfrac{2}{3}\eta\cos\left[\dfrac{4\pi}{3}(x+y+z)\right] & p=1 \\ \dfrac{1}{3} + \dfrac{2}{3}\eta\cos\left[\dfrac{4\pi}{3}(x+y+z)\right] & p=2 \\ \dfrac{1}{3} + \dfrac{2}{3}\eta\cos\left[\dfrac{4\pi}{3}(x+y+z)\right] & p=3, \end{cases}$$
$$\boldsymbol{R} = (x,y,z). \tag{14}$$

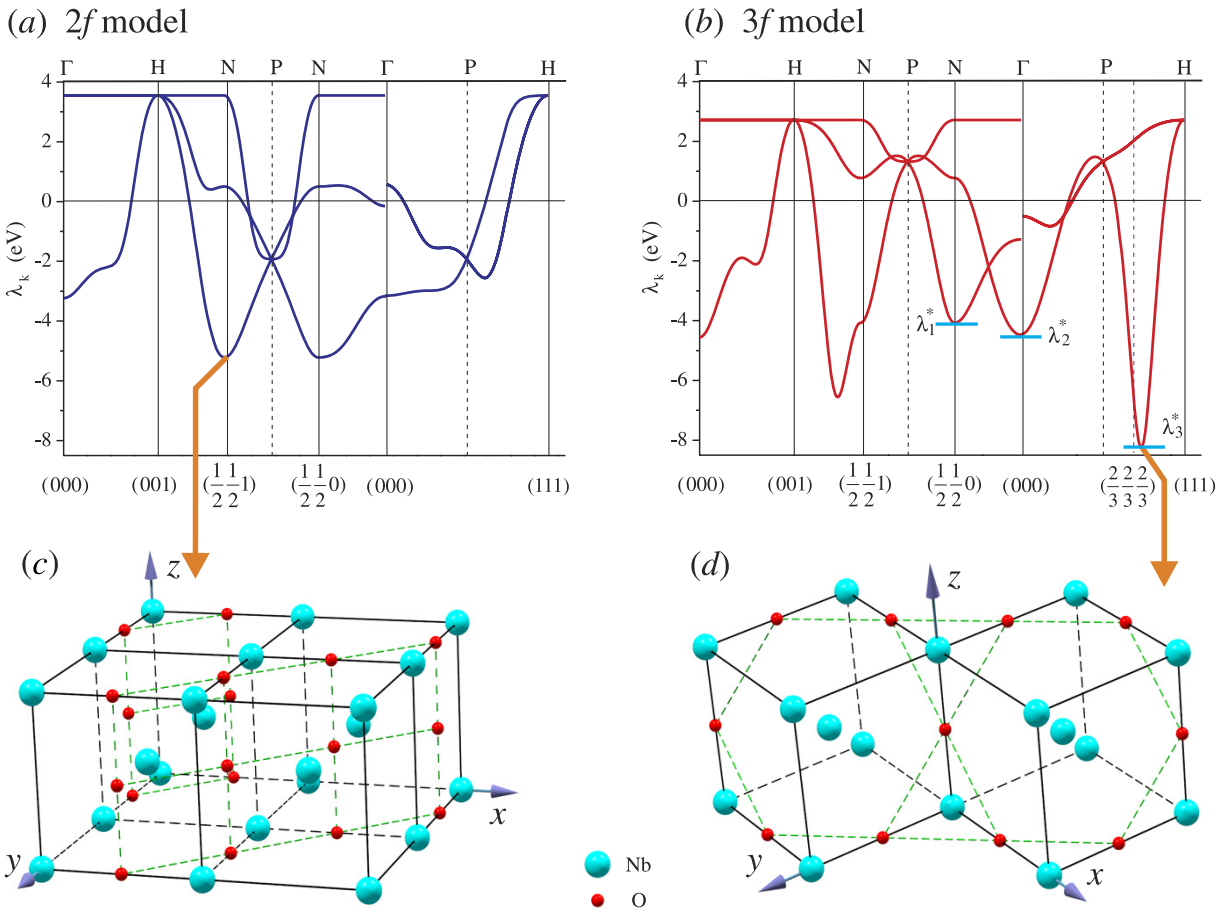

Figure 3. (*a*), (*b*) Eigenvalues λ_k of the matrix V^{si}_{pq} for two force models. Superstructure which corresponds to the (*c*) minimum $\lambda_{(\frac{1}{2},\frac{1}{2},0)}$ for the 2f model, (*d*) minimum $\lambda_{(\frac{2}{3},\frac{2}{3},\frac{2}{3})}$ for the 3f model.

One readily finds that $n(p, \boldsymbol{R})$ can be cast into the form

$$n(p,\boldsymbol{R}) = \begin{cases} c + 2c\cdot\cos\left[\dfrac{4\pi}{3}(x+y+z)\right] & p=1 \\ c + 2c\cdot\cos\left[\dfrac{4\pi}{3}(x+y+z)\right] & p=2 \\ c + 2c\cdot\cos\left[\dfrac{4\pi}{3}(x+y+z)\right] & p=3. \end{cases} \tag{15}$$

for any concentration $c < \frac{1}{3}$ (with $\eta = 3c$).

Figure 3(*d*) illustrates the obtained incommensurate superstructure with oxygen layers in the [111] direction, which has the same stoichiometric composition as the commensurate one but its atomic arrangement is formed by alternating (110) planes (figure 3(*c*)).

Within linear response theory the static displacement field $\boldsymbol{U}(\boldsymbol{R})$ reads [15, 19],

$$\boldsymbol{U}(\boldsymbol{R}) = 3c\sum_{\sigma,\boldsymbol{k}_s}\boldsymbol{G}(\boldsymbol{k}_s)\sum_{p}\boldsymbol{F}(p,\boldsymbol{k}_s)\upsilon_\sigma(p,\boldsymbol{k}_s)\gamma_\sigma(\boldsymbol{k}_s)\mathrm{e}^{-\mathrm{i}\boldsymbol{k}_s\boldsymbol{R}}. \tag{16}$$

Equation (16) is valid within the concentration range 0–4.2 at.% O, in which the Nb lattice parameter a_0 depends linearly on the O concentration [14]. We find that the superstructure (15) modulates the static displacement field (16) in such a way that two neighbouring (111) planes (which do not contain O) move towards each other by a displacement $\boldsymbol{U}_{[111]} = \pm 0.316 a_0 c(1,1,1)$, while each third (111) plane (which contains O) remains unmoved (see figure 4). Such a topology of the static displacement field is well known as a precursor for the ω phase formation [25–28]. Note that the fully collapsed ω phase is described by a displacement $\boldsymbol{U}^*_{[111]} = \pm a_0/12(1,1,1)$.

Within the mean-field approximation the critical (spinodal) temperature T_c of an order–disorder transition can be related to the energy minimum $\lambda^*(\boldsymbol{k})$ of a given superstructure by

$$T_c = -\frac{1}{k_B}c(1-c)\lambda^*(\boldsymbol{k}). \tag{17}$$

By identifying the energy value with $\lambda^*_1(\boldsymbol{k}) = -4.08$ eV and $\lambda^*_3(\boldsymbol{k}) = -8.25$ eV associated with the commensurate and incommensurate ordering wave (see figure 3(*b*)) the transition temperatures have been estimated for low oxygen concentrations. The calculated phase separation temperatures are associated with the energy minimum at the Γ point ($\lambda^*_2(\boldsymbol{k}) = -4.48$ eV), and can be interpreted as a solubility limit of atomic oxygen in Nb. Using (17) we calculated the phase boundaries of the commensurate and incommensurate ordering wave as well as the oxygen solubility limit. Figure 5

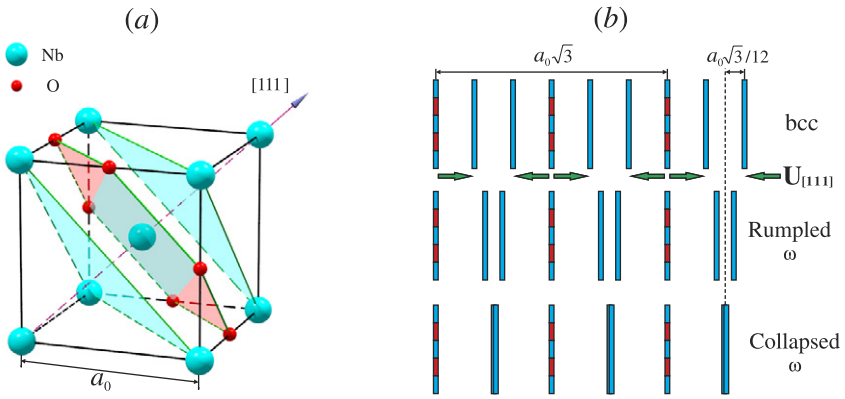

Figure 4. Atomic displacements in the ordered state: (*a*) bcc unit cell with three adjacent (111) planes; (*b*) formation of the ω phase. The atomic planes which do not contain oxygen are of shaded (blue), while the planes which contain oxygen are dashed-shaded (red).

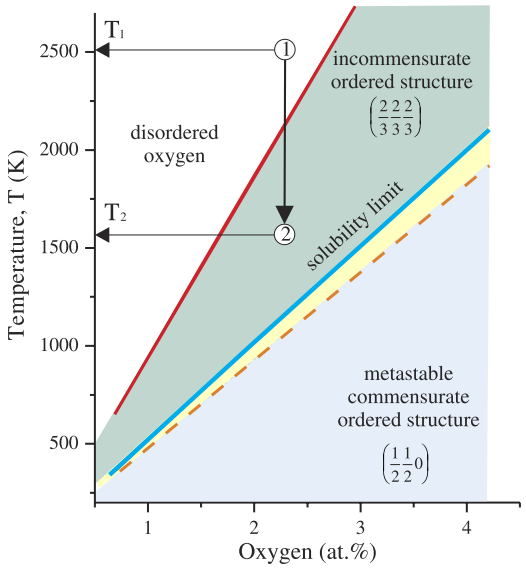

Figure 5. Relevant part of the mean-field Nb–O phase diagram at low oxygen concentrations displaying the calculated solubility limit line and the order–disorder phase transition lines for the superstructures which are associated with the positions of the minimum at $\boldsymbol{k} = (2/3, 2/3, 2/3)$ and $\boldsymbol{k} = (1/2, 1/2, 0)$ of the eigenvalue spectrum in figure 3(*b*).

shows the result of this rather straightforward calculation. It predicts the existence of a new phase above the solubility limit in which the incommensurate oxygen ordering wave is thermodynamically stable, while the commensurate ordering wave occurs below the solubility limit, thus is metastable (dashed line). It is interesting to note that the incommensurate oxygen ordering has never been observed. In fact, all experiments carried out so far have only reported indications of the metastable commensurate oxygen phase [7, 8]. Apparently, the oxygen uptake conditions have been such that the system was quenched into a metastable phase. From this theoretical study we predict that the incommensurate ordering wave should be observed if Nb is loaded with oxygen at a high temperature T_1 and then slowly cooled below the phase transition line T_2. It would also be interesting to investigate how the different O ordering states affect the superconducting properties of the Nb matrix.

References

[1] Lilje L *et al* 2004 *Nucl. Instrum. Methods Phys. Res.* A **516** 213
[2] Lilje L *et al* 2004 *Nucl. Instrum. Methods Phys. Res.* A **524** 1
[3] Ciovati G 2006 *Appl. Phys. Lett.* **89** 022507
[4] Delheusy M, Stierle A, Kasper N, Kurta R P, Vlad A, Dosch H, Antoine C, Resta A, Lundgren E and Andersen J 2008 *Appl. Phys. Lett.* **92** 101911
[5] Wiik B H 1997 *Nucl. Instrum. Methods Phys. Res.* A **398** 1
[6] DeSorbo W 1963 *Phys. Rev.* **132** 107
[7] Hellwig O, Becker H W and Zabel H 2001 *Phys. Rev.* B **64** 23
[8] Hellwig O and Zabel H 2003 *Physica* B **336** 90
[9] Blanter M S and Khachaturyan A G 1979 *Phys. Status Solidi* a **51** 291
[10] Dosch H, von Schwerin A and Peisl J 1986 *Phys. Rev.* B **34** 1654
[11] Dosch H and Peisl J 1985 *Phys. Rev.* B **32** 623
[12] Kanzaki H 1957 *J. Phys. Chem. Solids* **2** 24
[13] Tewary V K 1973 *Adv. Phys.* **22** 757
[14] Gebhardt E and Rothenbacher R 1963 *Z. Metalk.* **54** 443
[15] Khachaturyan A G 1983 *Theory of Structural Transformations in Solids* (New York: Wiley)
[16] Born M and Huang K 1954 *Dynamical Theory of Crystal Lattices* (Oxford: Clarendon)
[17] Cochran W 1954 *Phonons in Perfect Lattices and in Lattices With Point Imperfections (1965, Scottish Universities' Summer School)* ed R W H Stevenson (Edinburgh: Oliver and Boyd) p 53
[18] De Fontaine D 1979 *Solid State Phys.* **34** 73
[19] Khachaturyan A G and Pokrovskii B I 1985 *Prog. Mater. Sci.* **29** 1
[20] Khachaturyan A G 1973 *Phys. Status Solidi* b **60** 9
[21] Nakagawa Y and Woods A D B 1963 *Phys. Rev. Lett.* **11** 271
[22] Blanter M S and Khachaturyan A G 1978 *Metall. Trans.* A **9** 753
[23] Bugaev V N and Chepulskii R V 1995 *Phys. Status Solidi* b **192** 9
[24] Bugaev V N and Chepulskii R V 1995 *Acta Crystallogr.* A **52** 198
[25] De Fontaine D 1970 *Acta Metall.* **18** 275
[26] De Fontaine D 1988 *Metall. Trans.* A **18** 169
[27] Silcock J M 1958 *Acta Metall.* **6** 481
[28] Bagaryatskii Y A, Nosova G I and Tuganova T V 1955 *Dokl. Akad. Nauk SSSR* **105** 1225